Journal of Materials Chemistry C

PAPER

View Article Online
View Journal | View Issue

Cite this: J. Mater. Chem. C, 2016, 4, 9544

Resistive switching controlled by the hydration level in thin films of the biopigment eumelanin†

E. Di Mauro,[a] O. Carpentier,[a] S. I. Yáñez Sánchez,[a] N. Ignoumba Ignoumba,[a] M. Lalancette-Jean,[a] J. Lefebvre,[a] S. Zhang,[b] C. F. O. Graeff,[c] F. Cicoira[b] and C. Santato*[a]

Received 4th July 2016,
Accepted 21st September 2016

DOI: 10.1039/c6tc02793h

www.rsc.org/MaterialsC

Melanins are biopigments ubiquitous in flora and fauna, exhibiting a range of interesting functional properties such as UV-Vis photoprotection, thermoregulation, hydration-dependent electrical conduction and metal chelation. In the human body, melanins can be found in the skin, hair, middle ear, retina and heart. The metal chelation properties of neuromelanin, a subclass of melanins found in the dopaminergic neurons of the brain, may be involved in Parkinson's disease. Considering synthetic and natural (from the ink sac of the cuttlefish) thin films of eumelanin, the subclass of melanins most investigated by materials scientists, we report on two types of resistive switching (standard and hybrid), with different ON/OFF ratios, observed in planar gold/eumelanin/gold structures. The resistive switching process, based on the formation of conductive filaments, was studied by means of transient electrical measurements, scanning electron microscopy, atomic force microscopy and time of flight-secondary ion mass spectrometry. We observed an extended correlation among the factors affecting the two different types of switch: primarily the eumelanin's hydration level as well as the presence of chelating groups in the eumelanin molecular structure and the electrical bias. This work contributes to the development of environmentally benign organic resistive switching devices, namely electrochemical metallization memory cells making use of the biocompatible, biodegradable and abundant eumelanin biopigment as the ion conductive layer.

Introduction

Melanins are abundant pigments in the biosphere,[1] endowed with a vast set of interesting properties, notably thermoregulation, photoprotection, metal ion-chelation, and free radical quenching,[2] as well as antioxidant functions.[3]

Eumelanin is a black-brown subgroup of melanins,[4] whose building blocks are 5,6-dihydroxyindole (DHI) and 5,6-dihydroxyindole-2-carboxylic acid (DHICA).[2,5,6] Between four and eight of these building blocks form planar, covalently-bonded oligomers (protomolecules), which stack non-covalently *via* π–π interactions.[5,7–10] Its humidity dependent electrical conductivity, once studied in the context of amorphous semiconductivity,[11] has been recently reinterpreted as an electronic-ionic (protonic) mixed conduction.[1,12] Other intriguing features are radioprotection,[13] immunomodulatory activity,[14] biodegradability and biocompatibility.[15]

In humans, eumelanin can be found in the skin, hair, middle ear, retina and heart.[16,17]

Considerable attention has been paid to the involvement of eumelanin in the accumulation and release of metal cations in the human body.[18–21] Zinc,[18,20,22–27] copper,[22,23,25,26,28–30] calcium,[27,31,32] manganese,[33,34] iron and heavy metals[25,26,35–39] bind *in vivo* to eumelanins. Depending on the pH and the type of eumelanin (natural or synthetic), the phenolic hydroxyls, amine or carboxylic groups of the indolic building blocks have been reported to be preferential binding sites for metal cations.[40,41] Particular efforts have been made to understand the binding of iron to neuromelanin,[42–51] a subclass of melanin that accumulates within the dopaminergic neurons of the substantia nigra of the brain,[52] since iron has been reported in such neurons only in the case of Parkinson's disease.[53]

While the interactions of eumelanin with free metal cations have been extensively studied,[54] only recently attention has been paid to the interfaces between thin films of the pigment and metal electrodes,[55] mainly due to the well-known limited solubility of eumelanin in common organic solvents.[56]

[a] Department of Engineering Physics, Polytechnique Montréal, C.P. 6079, Succ. Centre-ville, Montréal, Québec, H3C 3A7, Canada. E-mail: clara.santato@polymtl.ca
[b] Department of Chemical Engineering, Polytechnique Montréal, C.P. 6079, Succ. Centre-ville, Montréal, Québec, H3C 3A7, Canada
[c] DF-FC, Universidade Estadual Paulista, Av. Eng. Luiz Edmundo Carrijo Coube 14-01, 17033-360, Bauru, Brazil

† Electronic supplementary information (ESI) available: AFM and SEM images, as well as further graphics. See DOI: 10.1039/c6tc02793h

The formation of tree-shaped electrically conductive bridges (dendrites) has been observed in hydrated eumelanin thin films included between gold electrodes, in planar configuration, under electrical bias.[55] Dendrites form by the dissolution of the positively biased Au electrode and migration of gold nanoclusters to the negative electrode, where they are reduced, forming dendrites, which grow towards the positive electrode. A dramatic drop in the resistivity takes place when the first dendrite bridges the electrodes (resistive switch, RS).[55]

Electrochemical metallization memory cells (ECMs), also called conductive bridge random access memories,[57] are a class of Resistive Random Access Memories (ReRAM),[58,59] which in turn are non-volatile memories.[59] The working mechanism of ECM is based on the formation of conductive filaments under bias: the active electrode dissolves generating cations that migrate through a solid electrolyte (ion conductor) to be reduced at the counter electrode, where the conductive filament nucleates.[59] The prospects of ReRAMs are low power consumption,[58,60–62] good reliability[57] as well as fast response time,[57,60] multilevel data storage[57,60,63] and high density.[58] Furthermore, filamentary-based systems can lead to nanoscale memory devices, because the switching takes place in highly localized regions, highlighting the ease of miniaturization.[64] Organic and polymeric switching memories, a subclass of ReRAMs, have become an emerging technology that could complement conventional memory technologies.[65–68] They feature advantages such as stackability,[69] scalability,[70] flexibility,[71–78] optical transparency,[73] printability[70,71] and offer the possibility of tuning electrical and physical properties by means of molecular design and chemical synthesis[79,80] for low-cost[81] and high density[59,82] memory applications. Organic polymers, possibly including salts, well-established organic electronics polymers and small molecules have been used in conductive bridge memories.[78,81,83–94]

Recently, interest in biomaterials for memories has increased in the context of green (sustainable) or biocompatible electronics.[95] Silk fibroin,[95–98] egg albumen,[99] cellulose,[75] chitosan doped with Ag[74,77] are examples of biomaterials that have been used in cells with conductive filament resistive switching. Interestingly, eumelanin presents both ion conduction[100] and metal binding properties,[54] features that promote the formation of metal filaments in polymers included between metal electrodes.[67]

The analogies between the phenomenon of dendrite growth in eumelanin films and the working mechanism of ECMs hints that the elucidation of metal–eumelanin interactions under bias may open technologically oriented studies *e.g.* where eumelanin can be used as ion conductor in ECMs with its characteristics of biodegradability[15] and biocompatibility.[56]

In this work, we report on transient electrical measurements in planar configuration on eumelanin thin films (Au/eumelanin/Au systems) at different experimental conditions, such as different relative humidity (RH) levels and hydration times. Planar systems are crucial for the investigation of the filament growth and, consequently, for the future development of stacked (vertical) resistive switching devices.[84] Scanning electron microscopy (SEM), atomic force microscopy (AFM) and time of flight-secondary ion mass spectrometry (ToF-SIMS) gave insights on the morphology and chemical composition of the filaments that formed in the hydrated films upon electrical bias as well as on the different types of resistive switch observed.

Experimental

Sample preparation

Synthetic (Sigma) eumelanin and natural (Sepia) eumelanin (extracted from the ink sac of a cuttlefish) were purchased from Sigma Aldrich (Canada) and had a chloride Cl^- content of respectively 0.83 ± 0.04 wt% and 6.92 ± 0.35 wt%, as measured by nuclear activation analysis (NAA). DMSO–melanin was synthesized by the group of Prof. C. Graeff, São Paulo State University – UNESP following a procedure reported in the literature[101] (chloride Cl^- content of 0.10 ± 0.01 wt%, as measured by NAA).

Eumelanin was dissolved in dimethyl sulfoxide (DMSO) sonicated and filtered (0.1 μm PTFE membrane with polypropylene housing, 25 mm diameter, PURADISC™), to yield suspensions of 15 mg mL^{-1}, approximately (as some eumelanin aggregates may have been trapped in the filter). NaCl was added to some of the 15 mg mL^{-1} suspensions of eumelanin in DMSO in concentrations of 0.8 mg mL^{-1} and 1.8 mg mL^{-1} (Table S1, ESI†).

The substrates (SiO_2 on Si) were purchased from Silicon Quest International (San Jose, California, USA), thickness 525 ± 25 μm. The Au electrodes were deposited by e-beam evaporation and photolithographically patterned on the substrates (5 nm of Ti as the adhesion layer and 30 nm of Au). The width of the electrodes was 4 mm, and the interelectrode distance was 10 μm. Prior to film deposition, the patterned substrates were cleaned in an ultrasonic bath with acetone, isopropanol, and de-ionized water, and then underwent a 10 min UV-ozone treatment. The thin films were spin coated (1 minute at 1000 rpm followed by 30 seconds at 4000 rpm) and hydrated in a Cole-Parmer mini humidify/dehumidify chamber (03323-14), which includes an automatic humidity controller and an ultrasonic humidification system. Controlled humidity ranged from 5 to 95% with programmable controller set-points.

Electrical measurements

The electrical measurements were performed with a Source Measure Unit (SMU), Agilent 2900A, with Quick IV Software for data recording. The confinement of the DMSO drops during transient current measurements was achieved by means of a well of polydimethylsiloxane (PDMS). The evaluation of the resistance after 5–10 months of storage was made with voltage sweeps (each cycle included three ramps: 0 V – maximum voltage, maximum voltage–minimum voltage, minimum voltage – 0 V) at combinations of the following conditions: 90% RH and at ambient RH (25%), at different sweep rates (0.2 mV s^{-1}, 2 mV s^{-1}, 200 mV s^{-1} and 2 V s^{-1}), in different voltage ranges (−1 V to 1 V, −2.5 V to 2.5 V, −5 V to 5 V, −10 V to 10 V), and, for the fastest sweep rates (200 mV s^{-1} and 2 V s^{-1}) for 10^2 cycles.

Other characterization techniques

Atomic force microscopy images were taken with a Dimension 3100 with Nanoscope V (Digital Instruments, Santa Barbara,

California, USA) with Si (model: ACTA) probes (tip radius <10 nm, spring constant 42 N m^{-1}) in tapping mode. The same microscope was used to measure the thickness: once a scratch had been done on the side of the interelectrode area, parallel to the channel, the thickness was then obtained from the profile of the scratch.

The measurements of the thickness by Spectral Reflectance were kindly carried out by the company Filmetrics (New York, USA), by means of a F40-Thin Film Analyzer.

Scanning electron microscopy was performed with a Microscope JEOL JSM7600F; all the images were taken in Secondary Electron Mode (SEM Voltage specified for each image). Samples were not metallized, unless otherwise stated. The EDX spectra were taken at the same microscope, Software: Aztec (Oxford), Detector: x-Max (80 mm^2) (Oxford), at 5 kV.

Raman measurements were carried out using a Renishaw Invia reflex confocal Raman microscope with a CCD detector. Raman spectra were collected at room temperature with 10% of maximum laser power, 30 s exposure time and five accumulations in static mode. A 1800 lines mm^{-1} grating was used in conjunction with 25 mW, 488 nm laser lines, focused on the samples using a 50× objective lens.

Nuclear activation analysis was performed with a SLOWPOKE nuclear reactor (Atomic Energy of Canada Limited) and a Ge semiconductor gamma-ray detector (Ortec, GEM55185). The samples were irradiated for 600 s at a thermal neutron flux of 5.4×10^{11} cm^{-2} s^{-1}. Gamma rays were detected after 120 s, for 600 s, at a distance of 35 mm. Time-of-flight secondary ion mass spectrometry (ToF-SIMS) analyses were performed using a TOF-SIMS IV (IONTOF, GmbH, Münster, Germany). Bi^{3+} cluster ions at 25 keV were used as primary ions in burst alignment mode to obtain high resolution ion mappings over areas of 50 μm × 50 μm. The pulsed ion current was 0.06 pA with a pulse width of 100 ns. Images were accumulated for 1000 s.

Results and discussion

Dendrite formation time

Transient current measurements performed at 1 V on films of synthetic eumelanin (hereinafter referred to as "Sigma eumelanin"), hydrated for 1 hour at 90% RH, revealed that, in about 40% of the cases, at least one dendrite bridged the interelectrode distance in a time range between 30 and 60 minutes. This standard resistive switch showed an ON/OFF ratio of $\sim 10^4$ (ratio between the electric current measured after (ON) and before (OFF) the electric resistive switch, Fig. S1, S2 and Table S2, ESI†). In the other cases, AFM and SEM images revealed that the process of dendrite formation was ongoing for biasing times longer than 1 hour. In particular, three different samples biased for times ≥ 3 hours (3 h, 15 h and 27 h) showed that the longer the biasing time, the closer was the sample to a resistive switch: after 15 hours, the dissolution of the positive electrode – and consequently the number of nanoclusters in the channel – was greater than after 3 hours and, after ≈ 28 hours, dendrites protruded from the negative electrode (Fig. 1).

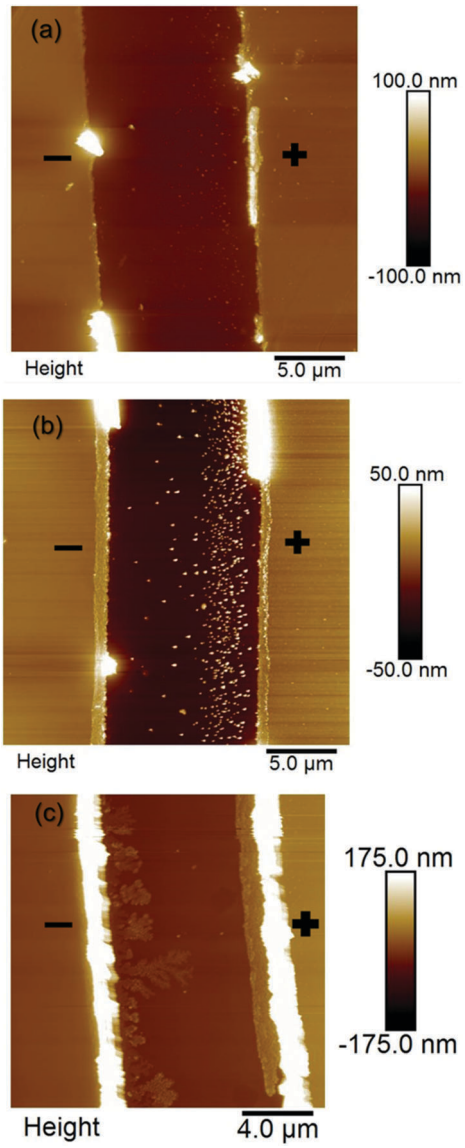

Fig. 1 AFM images: (a) 25 μm × 25 μm, interelectrode area of a thin film of Sigma melanin, hydrated for 1 hour at 90% RH and biased at 1 V for 3 hours: nanoclusters form; (b) 25 μm × 25 μm, interelectrode area of a thin film of Sigma eumelanin, hydrated for 1 hour at 90% RH and biased at 1 V for 15 hours: nanoclusters migrate towards the negative electrode; (c) 18 μm × 18 μm, interelectrode area of a thin film of Sigma melanin, hydrated for 1 hour at 90% RH and biased at 1 V for ≈ 28 hours: dendrites grow from the negative electrode towards the positive electrode.

Although the average thickness of the samples where a resistive switch took place in the first hour of bias (27 ± 7 nm) was higher than the average thickness of the remaining samples (18 ± 10 nm), we could rule out the thickness as a factor determining a higher probability of resistive switch, due to (i) the absence of a trend of the thickness with respect to the time to resistive switch (Fig. S3, ESI†) and (ii) samples having a thickness in the same range showing different biasing effects (*e.g.* for 3 samples with 30 nm thickness, we observed a resistive switch after half an hour, a resistive switch after one hour and material migration still ongoing after 15 hours).

The key parameter that likely differentiate the two sets of thin films (one with resistive switch in a time scale of 1 hour and the others with dendrite formation process still ongoing over time scales as long as 28 hours) is the suspension from which they were spin coated. We can tentatively hypothesize that the time required for dendrite formation dramatically depends on the local film morphology (that is, the arrangement of eumelanin nanoaggregates that make up the film), which may vary from sample to sample depending upon the nature of the suspension. Indeed, different suspensions of eumelanin in the solvent DMSO, at a concentration of 15 mg mL^{-1}, may include nanoaggregates with different supramolecular aggregation, size and shape,[102] due to the well-established limited solubility of eumelanin in common organic solvents.[56] In some cases, the local morphology of the thin films may be more favorable to gold nanocluster formation and migration than others, providing a preferential direction for the growth of the dendrite (straight rather than lateral) (Fig. S4, ESI†). We can conclude that, for thin films of Sigma eumelanin, the phenomenon of dendrite formation takes place in each sample but its kinetics cannot easily be foreseen.

Effects of the hydration time

In order to study the influence of the hydration time on the process of formation of the dendrites, transient current measurements were performed on thin films hydrated for times longer than 1 hour. The time frame between the fabrication of the thin film and the start of the electrical measurements, during which the thin film is exposed to a certain RH level and consequently absorbs water, plays a major role in the dendrite formation: the longer is time, the higher is the uptake of water, up to a saturation limit, with a logarithmic increase.[103] The water content is expected to have a dichotomous role: up to a certain amount, a favorable effect, in terms of faster migration of metal cations,[85] and above such amount a detrimental effect, in terms of instability (delamination) of the thin films.

A thin film obtained from the same suspensions that yielded slow dendrite formation was hydrated for $4\frac{1}{2}$ days at 90% RH (instead of 1 h). The length of the largest dendrites was one half of the ones observed in a thin film hydrated for 1 hour (Fig. S5, ESI†). Between 1 hour of hydration and $4\frac{1}{2}$ days, the logarithmic law that describes the water uptake for Sigma eumelanin powders at 90% RH[103] predicts that the water content increases from approximately 13 wt% to 19 wt% We tentatively propose that this increase in the water content triggers the onset of the destabilization of the films, in turn explaining the slower process.

The delamination phenomenon could also explain why a thin film with a hydration time of 14 days (water content foreseen of 21 wt%) does not show any dissolution of the positive electrode (Fig. S6, ESI†).

Effects of chloride content and eumelanin type (natural eumelanin and DMSO–melanin)

In order to investigate the influence of the chloride content, expected to play a role in the dissolution of the gold electrodes and intrinsically present in biological materials, transient current measurements were performed on thin films of Sigma eumelanin after addition of chlorides (Sigma eumelanin as received contains moderate amounts of chlorides, approximately 1 wt%). Intermediate and high chloride contents, respectively 4 wt% and 8 wt%, were considered (Table S1, ESI†). In contrast to as-received Sigma eumelanin, the time to resistive switch ranged between 6 and 14 minutes for films with intermediate Cl^- amount and between 2 and 7 minutes for thin films with high Cl^- amount. In this latter case, at points in the positive electrode facing dendrites growing from the negative electrode, it is visible that a dissolution is taking place, leaving ''coves'' (Fig. 2). The chemical composition in the coves is similar to that of films in the middle of the interelectrode region, as indicated by energy-dispersive X-ray spectroscopy (EDX). The EDX spectra show the same intensity of the peaks of C, Si and O, and a negligible Au peak (most likely due to the metallization layer) compared to areas where there are structures made of gold (such as the body of the dendrites and the electrodes). Furthermore, the coves are surrounded by gold-free holes resulting from the migration of the oxidized gold. As the border of the coves expand with the advancement of the oxidation of Au, such holes may eventually merge with the coves contributing to their growth. The presence of coves at the positive electrode is similar to recent observations for planar $Ag/AgClO_4$–PEO/Ag[87] and $Ag/AgClO_4$–PEO/Pt[84] systems. For thin films with high chloride content, a few cases of late resistive switching pointed again to the role played by the local morphology of the films on the switching process (Fig. S7 and S8, ESI†).

Transient current measurements at 1 V were also performed on Sepia eumelanin thin films. Sepia eumelanin has a content of Cl^- of about 7 wt%. As for synthetic eumelanin, the time to

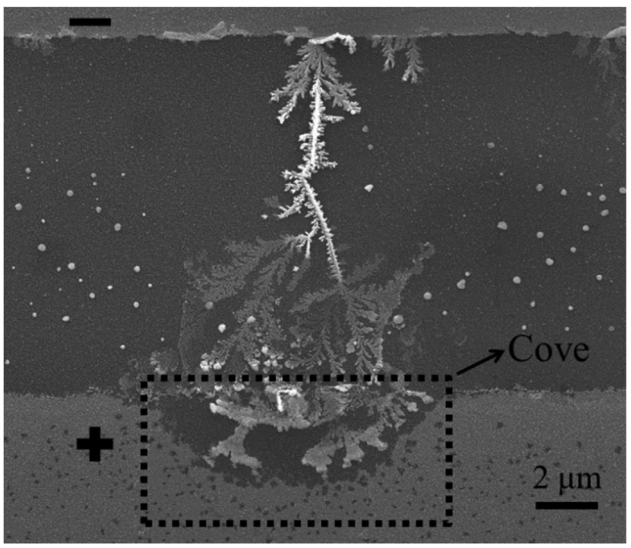

Fig. 2 SEM image of the dendrite bridging one electrode to the other in a thin film of Sigma eumelanin with high Cl^- content ($1\frac{1}{2}$ h hydration at 90% RH). The resistive switch took place after 3 minutes and the biasing voltage (1 V) was applied for 42 minutes. The sample was metallized (2 nm Au on the surface) prior to imaging. Image taken at 20 kV.

resistive switch varied depending on the suspension from which the thin film was spin coated (between 1.5 and 40 minutes). Sepia eumelanin thin films appeared to coexist with Sepia eumelanin granules (Fig. S9, ESI†), spherical or with a toroidal-like shape, with a bimodal size distribution (average diameters of 9 ± 3 μm and 2 ± 1 μm).[104,105] Such granules made the surface of Sepia eumelanin too rough for thickness measurements both by means of atomic force microscopy and spectral reflectance. Dendrites were observable within the interelectrode region in locations where granules were not present (Fig. S10, ESI†). It can be tentatively concluded that such granules are laying on a thin film of Sepia eumelanin. The film likely comprises fragments detached from the larger aggregates during the sonication; such a film was likely too thin to give a Raman spectroscopy signal but thick and continuous enough to promote the formation of the dendrites.

Sepia eumelanin showed, on average, longer times to resistive switch than Sigma eumelanin with high chloride content. As the two types of eumelanin have similar chlorides levels, this difference may be explained considering that Sepia eumelanin contains significant amounts of cations (Mg^{2+}, Ca^{2+}, Na^{+}[105] as well as K^{+}[106] and most of the first transition metals, especially Fe^{3+})[105,107] which may slow down the conductive bridge growth *e.g.* because the chelating sites may be already occupied.

Finally, it can be tentatively stated that the higher the chloride content, the more localized is the dissolution of the positive electrode and the faster is the resistive switch (Table S3, ESI†).

The role of the catecholic hydroxyl groups of eumelanin was elucidated replacing, as the material in the channel, Sigma eumelanin with DMSO–melanin (that partially lacks such groups)[101] with intermediate and high Cl^- levels. We found out that for biasing times as long as 12 hours there was no dissolution of the Au electrodes likely because of the low content of catecolic hydroxyl groups in DMSO–melanin (Fig. S11, ESI†).[101]

Concerning the effect of DMSO, the solvent used for film processing, transient current measurements carried out on drops of DMSO confined between Au electrodes revealed that a DMSO drop without any addition of Cl^- does not cause the dissolution of the positive electrode, for biasing times as long as 19 hours at 1 V (Fig. S12, ESI†). However, for amounts of Cl^- in DMSO similar to the high and intermediate amounts of Cl^- studied for Sigma eumelanin, nanostructures made of little spheres and composed by Au and C (as revealed by EDX) protrude from the negative electrode (Fig. S13, ESI†). As these nanostructures do not resemble trees (dendrites), this may point out that in DMSO the growth of nanostructures is not diffusion limited, as it happens in eumelanin thin films (Table S4, ESI†).

The combined effect of Cl^- and voltage

For a biasing voltage of 0.7 V, in the samples with intermediate Cl^- concentration, the positive electrode was not dissolved or there was very little dissolution. For thin films of Sigma eumelanin with high chloride content, the dendrite formation process takes place at voltages as low as 0.7 V: dendrites may be observed after 3 hours of electrical bias (Fig. 3). However, their morphology is different from that of dendrites formed at 1 V: their branches are very thin and very close together, to a point that the protruding structures have a bush-like, rather than a tree-like, shape.

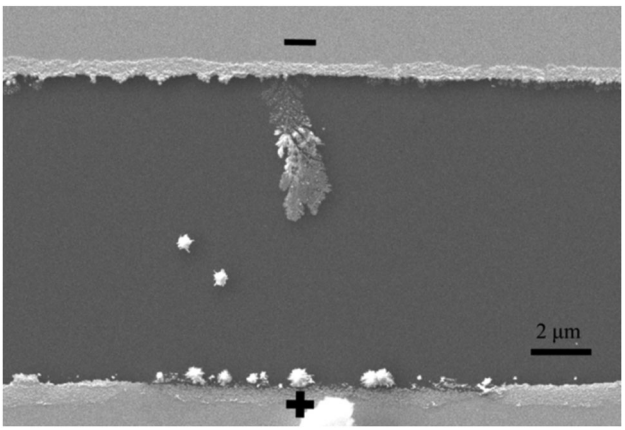

Fig. 3 SEM image of a dendrite growing in a thin film of Sigma melanin (8 wt% Cl^-), hydrated for 1 hour at 90% RH and biased at 0.7 V for 3 hours. No dendrite bridged the electrodes during the 3 hours of the measurement. Image taken at 10 kV.

The combined effect of Cl^- and hydration times longer than 1 hour

The slowing down effect of hydration treatments longer than one hour is also confirmed for thin films with an intermediate Cl^- amount in Sigma eumelanin. A thin film hydrated for five days showed only nanocluster formation, no dendrite growth and no resistive switch. Nevertheless, for films of Sigma eumelanin with high chloride concentration, both after three hours of hydration and 24 hours of hydration (water content of respectively 14.8 ± 0.1% and 16.7 ± 0.9 wt%),[103] a resistive switch takes place in the same time range of that of most of the thin films hydrated for one hour (2–7 minutes). Sepia eumelanin behaved differently. After 3 hours of bias, no dendrite bridged the electrodes (but several were growing) for a thin film hydrated for 3 hours. This is in agreement with the higher tendency of Sepia eumelanin to absorb H_2O (Fig. S15, ESI†), which may promote a destabilization of the thin film for hydration times shorter than for Sigma eumelanin.

Different ON/OFF ratios for different hydration levels

In order to shed further light on the effect of the water uptake on the process of dendrite formation, transient current measurements at constant biasing voltage, 1 V, were carried out at relative humidity levels lower than 90% and hydration time of one hour on thin films of Sigma eumelanin with high chloride content and Sepia eumelanin. In particular, 48%, 60%, 70% and 80% RH levels were tested.

At 70% and 80% RH (water content of approximately 10.3 ± 0.1%, and 10.8 ± 0.3%, respectively),[103] a new type of resistive switch was observed (Fig. 4). Whereas at 90% RH the ON/OFF ratio is $\sim 10^4$ (standard resistive switch), in this case the current increases by only 2–3 orders of magnitude

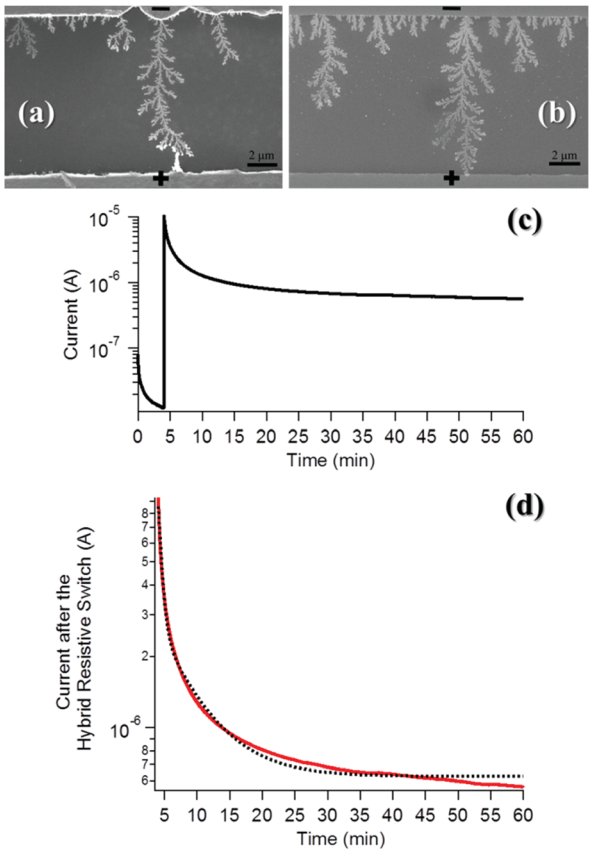

Fig. 4 (a) and (b) SEM images of dendrites bridging the two electrodes in two thin films of Sigma eumelanin (8 wt% Cl^-), hydrated for 1 hour at ≈80% RH and biased for 1 hour at 1 V. A hybrid resistive switch takes place after ≈4 minutes (a) and ≈12 minutes (b) of biasing. Images taken at 5 kV (a) and 10 kV (b); (c) current–time plot for sample (a); (d) zoom of the current–time diagram after the occurrence of the hybrid resistive switch: the dotted line represents the double exponential law that fits the trend $I(t) = I_0 + I_1 e^{[-(t - t_{rs})/\tau_1]} + I_2 e^{[-(t - t_{rs})/\tau_2]}$, where I_0 is 6.2554×10^{-7} A, I_1 is 5.8985×10^{-6} A, τ_1 is 0.553 min, I_2 is 2.0187×10^{-6} A, τ_2 is 5.892 min and t_{rs} is the time to the hybrid resistive switch (4.07 min).

(Table S2, ESI†) and then follows a double exponential decay with two different time constants (Fig. 4c). We call this new type of behavior hybrid resistive switch.

In order to confirm that the hybrid resistive switch was related to the water uptake, we performed a transient current measurement at 1 V on a thin film of Sigma eumelanin (Cl^- 8 wt%) that had been hydrated for only half an hour at 90% RH (with a water content expected to be within the range of water absorbed after 1 hour at 70% and 80% RH, Table S5, ESI†).[103] The results confirmed a hybrid resistive switch after 11 minutes of bias (Fig. S18, ESI†). Approximately 12 wt% (water content after one hour-hydration at 90% RH) can be taken as the threshold amount below which the dendrites do not show four orders of magnitude of current increase (standard resistive switch).

To shed light on the phenomenon of the hybrid resistive switch, time-of-flight secondary ion mass spectrometry (ToF-SIMS) was used, to investigate the dendrite composition. We computed (i) the ratios of the intensities of the peaks related to eumelanin fragments (C_xN, CNO, C_3NH, C_6, $C_yH_3NO_2$, x = [2,3,5,7], y = [4,6,8]) to the intensity of the peak related to Au (Au^-) and (ii) the peak intensity ratios MAu_x ($x \geq 2$)/MAu (where MAux is a eumelanin–Au complex, that is $CNAu_x$, $CNOAu_x$, C_3NAu_x, with $x \geq 2$). Both ratios (i) and (ii) were higher for the dendrite that showed a hybrid resistive switch than for the dendrite that caused a standard resistive switch (Fig. S19, Table S6 and S7, ESI†). In other words, the dendrites that sustained higher current contain purer gold. As a consequence, it can be hypothesized that the dendrites that caused a standard resistive switch are able to sustain a higher current because they contain a more continuous metal backbone, whereas the other type of dendrites is more of a hybrid metallic–organic structure.

Sepia eumelanin show a standard resistive switch at RH levels as low as 70%; this result confirms that it is the relative humidity (and, as a consequence, the water content) which is responsible for the two different types of ON/OFF ratios: indeed, at 70% RH Sepia eumelanin absorbs more water than synthetic eumelanin does at 90% RH for the same hydration time (Fig. S15, ESI†).[103] Results at RH levels lower than 70% are available in the ESI† (paragraph "Hydration at 48% and 60% RH", Fig. S16 and S17). A synoptic image of the phenomena taking place at the interface between gold electrodes and eumelanin thin films under electrical bias as well as details of the ON/OFF ratio for the two types of resistive switch are provided in Fig. 5 and Table S2 (ESI†).

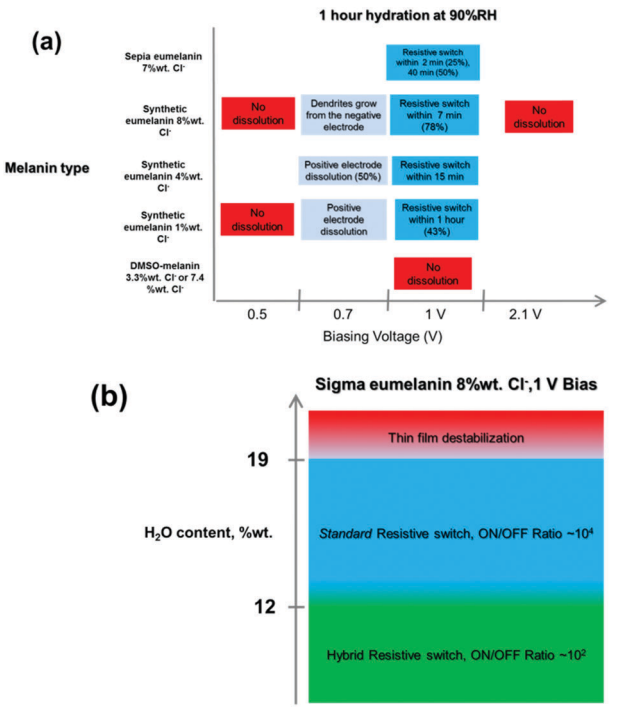

Fig. 5 (a) Diagram of the phenomena taking place at the interface between thin films of different types of eumelanin and gold electrodes, for 1 hour-hydration at 90% RH, at different biasing voltages (in parentheses the probability). (b) Scheme representing how the water level influences the type of resistive switch for Sigma eumelanin with 8 wt% Cl^-. Between approximately 12 wt% and 19 wt% a standard resistive switch occurs (ON/OFF ratio ~10^4); below 12 wt%, a hybrid resistive switch takes place (ON/OFF ratio ~10^2) whereas, above 19 wt%, the resistive switch is hindered by the thin film destabilization.

Attempt to erase the dendrites

For technological applications, the possibility of forming the conductive bridges is as important as that of annihilating them.

Attempts to erase the dendrites (that is, open them in order to interrupt the bridge between the electrodes) and bring the system back to the high resistive state were made. As the thin films of Sigma eumelanin with high chloride content had shown the best reproducibility in terms of time to resistive switch, they were used for the erasing attempt.

One test was chosen as representative: the thin film was hydrated for 1 hour at 90% RH, then biased for 12 minutes at 1 V (direct bias, during which the resistive switch occurred after 6 minutes) and finally for 12 hours at −1 V (reverse bias).

The dendrites were not erased by reversing the biasing voltage.

Nevertheless, some of them appeared partially consumed and discontinuous in some points along their bodies (Fig. S20, ESI†). The current during the reverse bias step was always of the order of mA (low resistive state after the resistive switch), confirming that only a fraction of the dendrites had been affected.

Moreover, some sides of the ''branches'' of the dendrites that were directly in front of the positive electrode after biasing voltage inversion look brighter in the SEM image, *i.e.* thicker, suggesting that the positive electrode after the biasing voltage inversion was dissolving and the material generated by its dissolution was accumulating on those branches (Fig. S20, ESI†). Small dendrites were nucleated on the negative electrode after biasing voltage inversion (Fig. S21, ESI†).

The results were confirmed by an experiment in which the dendrite formation was promoted by a sweeping (not constant) voltage (2 mV s^{-1}, initial and final voltage of each cycle = 0 V, max 2.5 V, min −2.5 V, 15 cycles), during which each electrode switched from positive to negative (and, consequently, from being the one consumed to the one towards which nanoclusters migrate) for 15 periods. In the interelectrode area dendrites protruding from both sides may be noted, some of which meet ''half way'' in the middle of channel. Rather than being akin to trees, these structures resemble leaves, perhaps due to the fact that they received nanoaggregates from both sides (both electrodes have been consumed) (Fig. S22, ESI†).

Retention time

In order to evaluate the retention time, *i.e.* how long the system remained in the low resistive state, the samples for which a resistive switch occurred were biased again, with voltage ramps, after a period of 5–10 months at ambient temperature and 25% RH.

The results revealed that samples are able to keep the low resistive state for a period of time as long as 10 months, showing a perfect ohmic behaviour, up to voltages as high as |10| V for films $\geq$ *ca.* 25 nm. The resistance of the low resistive state proved to not be influenced by the RH level, sweep rates, voltage range and number of cycles (up to 100). This hints to a potential application for Write Once Read-Many-Times (WORM)-type memories. For thicknesses below *ca.* 25 nm, the low resistive state was lost. The film thickness, which did not play a role on the time to resistive switch, plays conversely a major role in determining the retention time: it can be hypothesized that it protects the thin dendrites from degradation due to the contact with the ambient atmosphere. Samples with a hybrid resistive switch lost their high conductive state after 10 months in agreement with our ToF-SIMS results: as their dendrites contain more eumelanin than the other type of dendrites, we suggest that the degradation of the pigment[4] causes the loss of the low resistive state.

Conclusions

We have found that it is possible to obtain two types of resistive switch, standard (ON/OFF ratio $\sim 10^4$) and hybrid (ON/OFF ratio $\sim 10^2$), in thin films of the biopigment eumelanin, in planar electrochemical metallization cell configuration.

Using eumelanins from synthetic and natural (the ink sac of the cuttlefish, Sepia) sources, we have revealed the complex interplay of factors determining the resistive switch process. These factors are: eumelanin hydration level (depending on relative humidity and hydration time), chelating groups in the molecular structure of the pigment, electrical bias and content of chlorides (commonly present in biological environments and known to promote the formation of gold complexes). In particular, if the hydration level is below a lower threshold (12 wt%) the hybrid dendrites form. Between 12 and 19 wt%, we observe the standard resistive switch. For hydration levels higher than 19 wt%, the process is slower or does not take place. Our results pave the way towards the demonstration of the use of eumelanin as the ionic conductor in electrochemical metallization memory cells. With the aim to enhance the control over the cell switching characteristics, work is in progress to improve the chemical control of our eumelanin films, *e.g.* by solid state polymerization of the biopigment building block DHI.[108] Using a two-color electrode configuration (*e.g.* Pt and Au), we aim at demonstrating, in the near future, the possibility of erasing the dendrites. Nanoscale memory devices, with a vertical (stacked) configuration, are currently under investigation. In addition, the study of the interactions between eumelanin and metal electrodes may potentially shed light on the biological functions of the pigment as a metal ion chelator. Indeed, Sepia eumelanin has been proved to be a suitable model to study the binding properties of neuromelanin.[109] Therefore, the following steps of our research will be the inclusion of electrodes made of biologically relevant metals (such as Copper, Iron or Magnesium).

Acknowledgements

The authors are thankful to Prof. Arthur Yelon (Polytechique Montréal) and Prof. A. Pezzella (Università Federico II di Napoli) for fruitful discussions and to Yves Drolet for technical support during the electrical measurements. They acknowledge the technical support of N. MacDonald (CM2 research center)

with SEM microscopy, P. Moraille (GCM Université de Montréal/Polytechnique Montréal) with AFM microscopy and J. Coleman (Filmetrics) for thickness measurements by means of Spectral Reflectance. The microfabrication costs were partially covered by CMC Microsystems (MNT Grants). CS and FC acknowledge financial support by FQRNT (Équipe) and NSERC (Discovery Grants).

Notes and references

1 B. Mostert, B. J. Powell, F. L. Pratt, G. R. Hanson, T. Sarna, I. R. Gentle and P. Meredith, *Proc. Natl. Acad. Sci. U. S. A.*, 2012, **109**, 8943–8947.
2 G. Prota, *Melanins and Melanogenesis*, Academic Press, San Diego, 1992.
3 P. Meredith and T. Sarna, *Pigm. Cell Res.*, 2006, **19**, 572–594.
4 M. d'Ischia, K. Wakamatsu, A. Napolitano, S. Briganti, J. C. Garcia-Borron, D. Kovacs, P. Meredith, A. Pezzella, M. Picardo, T. Sarna, J. D. Simon and S. Ito, *Pigm. Cell Melanoma Res.*, 2013, **26**, 616–633.
5 G. W. Zajac, J. M. Gallas, J. Cheng, M. Eisner, S. C. Moss and A. E. Alvarado-Swaisgood, *Biochim. Biophys. Acta, Gen. Subj.*, 1994, **1199**, 271–278.
6 M. Arzillo, G. Mangiapia, A. Pezzella, R. K. Heenan, A. Radulescu, L. Paduano and M. D'Ischia, *Biomacromolecules*, 2012, **13**, 2379–2390.
7 A. A. R. Watt, J. P. Bothma and P. Meredith, *Soft Matter*, 2009, **5**, 3754.
8 G. W. Zajac, J. M. Gallas and A. E. Alvarado-Swaisgood, *J. Vac. Sci. Technol., B: Microelectron. Nanometer Struct.--Process., Meas., Phenom.*, 1994, **12**, 1512.
9 K. B. Stark, J. M. Gallas, G. W. Zajac, M. Eisner and J. T. Golab, *J. Phys. Chem. B*, 2003, **107**, 11558–11562.
10 C. M. R. Clancy and J. D. Simon, *Biochemistry*, 2001, **40**, 13353–13360.
11 J. McGinness, P. Corry and P. Proctor, *Science*, 1974, **183**, 853–855.
12 S. B. Rienecker, A. B. Mostert, G. Schenk, G. R. Hanson and P. Meredith, *J. Phys. Chem. B*, 2015, **119**, 14994–15000.
13 A. Kunwar, B. Adhikary, S. Jayakumar, A. Barik, S. Chattopadhyay, S. Raghukumar and K. I. Priyadarsini, *Toxicol. Appl. Pharmacol.*, 2012, **264**, 202–211.
14 V. M. Sava, B. N. Galkin, M.-Y. Hong, P.-C. Yang and G. S. Huang, *Food Res. Int.*, 2001, **34**, 337–343.
15 C. J. Bettinger, J. P. Bruggeman, A. Misra, J. T. Borenstein and R. Langer, *Biomaterials*, 2009, **30**, 3050–3057.
16 R. Crippa, V. Horak, G. Prota, P. Svoronos and L. Wolfram, *Alkaloids Chem. Pharmacol.*, 1990, **36**, 253–323.
17 S. Colombo, I. Berlin, V. Delmas and L. Larue, *Melanins and Melanosomes*, Wiley-VCH Verlag GmbH & Co. KGaA, Weinheim, Germany, 2011, pp. 21–61.
18 J. M. Bowness and R. A. Morton, *Biochem. J.*, 1953, **53**, 620–626.
19 B. J. Panessa and J. A. Zadunaisky, *Exp. Eye Res.*, 1981, **32**, 593–604.
20 J. Borovanský, *Sb Lek*, 1994, **95**, 309–320.
21 W. D. Bush and J. D. Simon, *Pigm. Cell Res.*, 2007, **20**, 134–139.
22 J. M. Bowness and R. A. Morton, *Biochem. J.*, 1952, **51**, 530–535.
23 J. Horcicko, J. Borovansky, J. Ducholi and B. Prochazkova, *Hoppe-Seyler's Zeitschrift für Physiol. Chemie*, 1973, **354**, 203–204.
24 M. Chatelain, J. Gasparini, L. Jacquin and A. Frantz, *Biol. Lett.*, 2014, **10**, 20140164.
25 W. D. Stein, *Nature*, 1955, **175**, 256–257.
26 J. Andrzejczak and E. Buszman, *Acta Biochim. Pol.*, 1992, **39**, 85–88.
27 L. Hong and J. D. Simon, *Photochem. Photobiol.*, 2005, **81**, 517–523.
28 H. M. Swartz, T. Sarna and L. Zecca, *Ann. Neurol.*, 1992, **32**, S69–S75.
29 P. Flesch, *Exp. Biol. Med.*, 1949, **70**, 79–80.
30 W. S. Enochs, M. J. Nilges and H. M. Swartz, *J. Neurochem.*, 1993, **61**, 68–79.
31 B. J. Panessa and J. A. Zadunaisky, *Exp. Eye Res.*, 1981, **32**, 593–604.
32 R. Salceda and G. Sánchez-Chávez, *Cell Calcium*, 2000, **27**, 223–229.
33 A. Lydén, B. S. Larsson and N. G. Lindquist, *Acta Pharmacol. Toxicol.*, 1984, **55**, 133–138.
34 G. C. Cotzias, P. S. Papavasiliou and S. T. Miller, *Nature*, 1964, **201**, 1228–1229.
35 B. S. Larsson, *Pigm. Cell Res.*, 1993, **6**, 127–133.
36 R. A. Nicolaus, *Rass. Med. Sper.*, 1962, **9**, 1–32.
37 B. Larsson and H. Tjälve, *Acta Physiol. Scand.*, 1978, **104**, 479–484.
38 L. P. White, *Nature*, 1958, **182**, 1427–1428.
39 M. Okazaki, K. Kuwata, Y. Miki, S. Shiga and T. Shiga, *Arch. Biochem. Biophys.*, 1985, **242**, 197–205.
40 L. Hong and J. D. Simon, *Photochem. Photobiol.*, 2006, **82**, 1265–1269.
41 M. d'Ischia, A. Napolitano, A. Pezzella, P. Meredith and T. Sarna, *Angew. Chem., Int. Ed.*, 2009, **48**, 3914–3921.
42 T. Shima, T. Sarna, H. M. Swartz, A. Stroppolo, R. Gerbasi and L. Zecca, *Free Radical Biol. Med.*, 1997, **23**, 110–119.
43 B. Larsson and H. Tjälve, *Biochem. Pharmacol.*, 1979, **28**, 1181–1187.
44 K. Jellinger, E. Kienzl, G. Rumpelmair, P. Riederer, H. Stachelberger, D. Ben-Shachar and M. B. H. Youdim, *J. Neurochem.*, 1992, **59**, 1168–1171.
45 D. Ben-Shachar, P. Riederer and M. B. H. Youdim, *J. Neurochem.*, 1991, **57**, 1609–1614.
46 M. B. H. Youdim, D. Ben-Shachar and P. Riederer, *Acta Neurol. Scand.*, 1989, **80**, 47–54.
47 S. Bohic, K. Murphy, W. Paulus, P. Cloetens, M. Salomé, J. Susini and K. Double, *Anal. Chem.*, 2008, **80**, 9557–9566.
48 L. Zecca, D. Tampellini, A. Gatti, R. Crippa, M. Eisner, D. Sulzer, S. Ito, R. Fariello and M. Gallorini, *J. Neural Transm.*, 2002, **109**, 663–672.
49 L. Zecca, M. Gallorini, V. Schünemann, A. X. Trautwein, M. Gerlach, P. Riederer, P. Vezzoni and D. Tampellini, *J. Neurochem.*, 2001, **76**, 1766–1773.

50 D. T. Dexter, F. R. Wells, A. J. Lee, F. Agid, Y. Agid, P. Jenner and C. D. Marsden, *J. Neurochem.*, 1989, **52**, 1830–1836.
51 E. C. Hirsch, J.-P. Brandel, P. Galle, F. Javoy-Agid and Y. Agid, *J. Neurochem.*, 1991, **56**, 446–451.
52 M. d'Ischia, A. Napolitano, V. Ball, C. Chen and M. J. Buehler, *Acc. Chem. Res.*, 2014, **47**, 3541–3550.
53 D. Ben-Shachar and M. B. H. Youdim, *Prog. Neuro-Psychopharmacol. Biol. Psychiatry*, 1993, **17**, IN3–IN150.
54 L. Hong and J. D. Simon, *J. Phys. Chem. B*, 2007, **111**, 7938–7947.
55 J. Wünsche, L. Cardenas, F. Rosei, F. Cicoira, R. Gauvin, C. F. O. Graeff, S. Poulin, A. Pezzella and C. Santato, *Adv. Funct. Mater.*, 2013, **23**, 5591–5598.
56 J. P. Bothma, J. De Boor, U. Divakar, P. E. Schwenn and P. Meredith, *Adv. Mater.*, 2008, **20**, 3539–3542.
57 W. Lu, D. S. Jeong, M. Kozicki and R. Waser, *MRS Bull.*, 2012, **37**, 124–130.
58 R. Waser, R. Dittmann, G. Staikov and K. Szot, *Adv. Mater.*, 2009, **21**, 2632–2663.
59 I. Valov, R. Waser, J. R. Jameson and M. N. Kozicki, *Nanotechnology*, 2011, **22**, 289502.
60 S. Tappertzhofen, I. Valov, T. Tsuruoka, T. Hasegawa, R. Waser and M. Aono, *ACS Nano*, 2013, **7**, 6396–6402.
61 N. Raghavan, *Microelectron. Reliab.*, 2014, **54**, 2253–2257.
62 F. Pan, C. Chen, Z. Wang, Y. Yang, J. Yang and F. Zeng, *Prog. Nat. Sci.: Mater. Int.*, 2010, **20**, 1–15.
63 J. Qi, M. Olmedo, J.-G. Zheng and J. Liu, *Sci. Rep.*, 2013, **3**, 2405.
64 B. Cho, S. Song, Y. Ji, T.-W. Kim and T. Lee, *Adv. Funct. Mater.*, 2011, **21**, 2806–2829.
65 J. C. Scott and L. D. Bozano, *Adv. Mater.*, 2007, **19**, 1452–1463.
66 W.-P. Lin, S.-J. Liu, T. Gong, Q. Zhao and W. Huang, *Adv. Mater.*, 2014, **26**, 570–606.
67 Q.-D. Ling, D.-J. Liaw, C. Zhu, D. S.-H. Chan, E.-T. Kang and K.-G. Neoh, *Prog. Polym. Sci.*, 2008, **33**, 917–978.
68 Q.-D. Ling, D.-J. Liaw, E. Y.-H. Teo, C. Zhu, D. S.-H. Chan, E.-T. Kang and K.-G. Neoh, *Polymer*, 2007, **48**, 5182–5201.
69 S. Song, B. Cho, T.-W. Kim, Y. Ji, M. Jo, G. Wang, M. Choe, Y. H. Kahng, H. Hwang and T. Lee, *Adv. Mater.*, 2010, **22**, 5048–5052.
70 J. J. Kim, B. Cho, K. S. Kim, T. Lee and G. Y. Jung, *Adv. Mater.*, 2011, **23**, 2104–2107.
71 Y. Ji, B. Cho, S. Song, T.-W. Kim, M. Choe, Y. H. Kahng and T. Lee, *Adv. Mater.*, 2010, **22**, 3071–3075.
72 L. Li, Q.-D. Ling, S.-L. Lim, Y.-P. Tan, C. Zhu, D. S. H. Chan, E.-T. Kang and K.-G. Neoh, *Org. Electron.*, 2007, **8**, 401–406.
73 H.-D. Kim, M. J. Yun, J. H. Lee, K. H. Kim and T. G. Kim, *Sci. Rep.*, 2014, **4**, 4614.
74 N. R. Hosseini and J.-S. Lee, *Adv. Funct. Mater.*, 2015, **25**, 5586–5592.
75 K. Nagashima, H. Koga, U. Celano, F. Zhuge, M. Kanai, S. Rahong, G. Meng, Y. He, J. De Boeck, M. Jurczak, W. Vandervorst, T. Kitaoka, M. Nogi and T. Yanagida, *Sci. Rep.*, 2014, **4**, 5532.
76 H. Wang, F. Meng, Y. Cai, L. Zheng, Y. Li, Y. Liu, Y. Jiang, X. Wang and X. Chen, *Adv. Mater.*, 2013, **25**, 5498–5503.
77 N. Raeis Hosseini and J.-S. Lee, *ACS Nano*, 2015, **9**, 419–426.
78 S. R. Mohapatra, T. Tsuruoka, T. Hasegawa, K. Terabe and M. Aono, *AIP Adv.*, 2012, **2**, 022144.
79 Y.-P. Hsiao, W.-L. Yang, L.-M. Lin, F.-T. Chin, Y.-H. Lin, K.-L. Yang and C.-C. Wu, *Microelectron. Reliab.*, 2015, **55**, 2188–2197.
80 F. M. Raymo, *Adv. Mater.*, 2002, **14**, 401–414.
81 B. Cho, J.-M. Yun, S. Song, Y. Ji, D.-Y. Kim and T. Lee, *Adv. Funct. Mater.*, 2011, **21**, 3976–3981.
82 L. P. Ma, J. Liu and Y. Yang, *Appl. Phys. Lett.*, 2002, **80**, 2997.
83 Y. Busby, N. Crespo-Monteiro, M. Girleanu, M. Brinkmann, O. Ersen and J.-J. Pireaux, *Org. Electron.*, 2015, **16**, 40–45.
84 K. Krishnan, T. Tsuruoka, C. Mannequin and M. Aono, *Adv. Mater.*, 2016, **28**, 640–648.
85 S. R. Mohapatra, T. Tsuruoka, K. Krishnan, T. Hasegawa and M. Aono, *J. Mater. Chem. C*, 2015, **3**, 5715–5720.
86 S. Wu, T. Tsuruoka, K. Terabe, T. Hasegawa, J. P. Hill, K. Ariga and M. Aono, *Adv. Funct. Mater.*, 2011, **21**, 93–99.
87 K. Krishnan, T. Tsuruoka and M. Aono, *Jpn. J. Appl. Phys.*, 2016, **55**, 06GK02.
88 Y. Busby, S. Nau, S. Sax, E. J. W. List-Kratochvil, J. Novak, R. Banerjee, F. Schreiber and J.-J. Pireaux, *J. Appl. Phys.*, 2015, **118**, 075501.
89 F. Santoni, A. Gagliardi, M. A. der Maur, A. Pecchia, S. Nau, S. Sax, E. J. W. List-Kratochvil and A. di Carlo, *IEEE Trans. Nanotechnol.*, 2016, **15**, 60–69.
90 N. Knorr, A. Bamedi, Z. Karipidou, R. Wirtz, M. Sarpasan, S. Rosselli and G. Nelles, *J. Appl. Phys.*, 2013, **114**, 124510.
91 T. Graves-Abe and J. C. Stunn, *Dynamics of Write and Erase Mechanisms in a Novel Organic Memory With Extremely Low ON Resistance*, IEEE, 2005, 0-7803-904.
92 V. C. Nguyen and P. S. Lee, *Appl. Phys. Lett.*, 2016, **108**, 033301.
93 W.-J. Joo, T.-L. Choi, K.-H. Lee and Y. Chung, *J. Phys. Chem. B*, 2007, **111**, 7756–7760.
94 S. Gao, C. Song, C. Chen, F. Zeng and F. Pan, *J. Phys. Chem. C*, 2012, **116**, 17955–17959.
95 H. Wang, Y. Du, Y. Li, B. Zhu, W. R. Leow, Y. Li, J. Pan, T. Wu and X. Chen, *Adv. Funct. Mater.*, 2015, **25**, 3825–3831.
96 C. Mukherjee, M. K. Hota, D. Naskar, S. C. Kundu and C. K. Maiti, *Phys. Status Solidi*, 2013, 1797–1805.
97 M. K. Hota, M. K. Bera, B. Kundu, S. C. Kundu and C. K. Maiti, *Adv. Funct. Mater.*, 2012, **22**, 4493–4499.
98 B. Sun, D. Liang, X. Li and P. Chen, *J. Mater. Sci.: Mater. Electron.*, 2016, **27**, 3957–3962.
99 Y.-C. Chen, H.-C. Yu, C.-Y. Huang, W.-L. Chung, S.-L. Wu and Y.-K. Su, *Sci. Rep.*, 2015, **5**, 10022.
100 J. Wünsche, Y. Deng, P. Kumar, E. Di Mauro, E. Josberger, J. Sayago, A. Pezzella, F. Soavi, F. Cicoira, M. Rolandi and C. Santato, *Chem. Mater.*, 2015, **27**, 436–442.
101 E. S. Bronze-Uhle, A. Batagin-Neto, P. H. P. Xavier, N. I. Fernandes, E. R. De Azevedo and C. F. O. Graeff, *J. Mol. Struct.*, 2013, **1047**, 102–108.

102 S. Yue, G. C. Berry and R. D. McCullough, *Macromolecules*, 1996, **29**, 933–939.
103 L. G. Albano, E. Di Mauro, P. Kumar, F. Cicoira, C. F. Graeff and C. Santato, *Polym. Int.*, 2016, **26**, 19007–19013.
104 Y. Liu and J. D. Simon, *Pigm. Cell Res.*, 2003, **16**, 72–80.
105 A. Mbonyiryivuze, Z. Y. Nuru, L. Kotsedi, B. Mwakikunga, S. M. Dhlamini, E. Park and M. Maaza, *Mater. Today Proc.*, 2015, **2**, 3988–3997.
106 A. Mbonyiryivuze, Z. Y. Nuru, B. Diop Ngom, B. Mwakikunga, S. Mokhotjwa Dhlamini, E. Park and M. Maaza, *Am. J. Nanomater.*, 2015, **3**, 22–27.
107 Y. Liu and J. D. Simon, *Pigm. Cell Res.*, 2005, **18**, 42–48.
108 A. Pezzella, M. Barra, A. Musto, A. Navarra, M. Alfè, P. Manini, S. Parisi, A. Cassinese, V. Criscuolo and M. d'Ischia, *Mater. Horiz.*, 2015, 212–220.
109 R. L. Schroeder, K. L. Double and J. P. Gerber, *J. Chem. Neuroanat.*, 2015, **64–65**, 20–32.